

Reliable Vertical Ground Reaction Force Estimation with Smart Insole During Walking

Femi Olugbon, Nozhan Ghoreishi, Ming-Chun Huang, Wenyao Xu, and Diliang Chen

Abstract—The vertical ground reaction force (vGRF) and its characteristic weight acceptance and push-off peaks measured during walking are important for gait and biomechanical analysis. Current wearable vGRF estimation methods suffer from drifting errors or low generalization performances, limiting their practical application. This paper proposes a novel method for reliably estimating vGRF and its characteristic peaks using data collected from the smart insole, including inertial measurement unit data and the newly introduced center of the pressed sensor data. These data were fused with machine learning algorithms including artificial neural networks, random forest regression, and bi-directional long-short-term memory. The proposed method outperformed the state-of-the-art methods with the root mean squared error, normalized root mean squared error, and correlation coefficient of 0.024 body weight (BW), 1.79% BW, and 0.997 in intra-participant testing, and 0.044 BW, 3.22% BW, and 0.991 in inter-participant testing, respectively. The difference between the reference and estimated weight acceptance and push-off peak values are 0.022 BW and 0.017 BW with a delay of 1.4% and 1.8% of the gait cycle for the intra-participant testing and 0.044 BW and 0.025 BW with a delay of 1.5% and 2.3% of the gait cycle for the inter-participant testing. The results indicate that the proposed vGRF estimation method has the potential to achieve accurate vGRF measurement during walking in free-living environments.

Index Terms—Gait analysis, ground reaction force, inertial measurement unit (IMU), center of the pressed sensor, walking.

I. INTRODUCTION

THE vertical ground reaction force (vGRF) is the dominant component of the ground reaction force during walking, which plays an important role in human biomechanical studies, providing essential data for estimating kinematics and kinetic gait parameters [1]–[3].

The vGRF has been measured or estimated using a variety of methods in clinical and real-life scenarios. In the traditional vGRF measurement methods, in-ground force plates and force-plate integrated treadmills are commonly used to analyze human gait due to their high accuracy, reproducibility, and reliability [4]. However, their complexity and size limit their applications to confined laboratory and clinical settings.

Manuscript received April xx, 20xx; revised August xx, 20xx. (Corresponding author: Diliang Chen.)

Femi Olugbon, Nozhan Ghoreishi, and Diliang Chen are with the Department of Electrical and Computer Engineering, University of New Hampshire, Durham, NH 03824 USA (e-mail:femi.olugbon@unh.edu, nozhan.ghoreishi@unh.edu, diliang.chen@unh.edu), Ming-Chun Huang is with the Department of Data and Computational Science, Duke Kunshan University, Suzhou, China (e-mail:mh596@duke.edu), Wenyao Xu is with the Department of Computer Science & Engineering, University at Buffalo, the State University of New York, Buffalo, NY 14260 USA (e-mail:wenyaoxu@buffalo.edu)

The limitations of traditional vGRF measurement methods restrict their applications in real-life scenarios, such as remote monitoring of patients, performance analysis of athletes, and gait analysis for activities of daily living where accurate vGRF measurements are required. Also, complex activities such as stairs and ramp ascent and descent usually require expensive setups that comprise multiple force plates, high-speed motion cameras, and complex signal processing software [5], [6].

To overcome the limitations of traditional vGRF measurement systems, wearable force sensing insole systems have been explored to achieve vGRF measurement in free-living environments [7]. Current designs of wearable pressure sensors use different sensing methods such as force-sensitive resistors (FSR) [8], resistive carbon polymers [9], and piezoresistive sensors [10] to measure continuous pressure values under the foot's surface. However, existing wearable insole systems require frequent calibrations due to sensor drift. This leads to inconsistent readings over time [11].

To address the limitations of wearable insole systems in measuring vGRF, several methods were developed to estimate vGRF indirectly from the kinematics of human body segments [12]. Inertial measurement units (IMU) have become popular in gait analysis research due to the advances in the development of small and wearable sensors capable of measuring the acceleration, angular velocity, and magnetic fields [13]. Previous studies have used IMU and human biomechanical models [14] and machine learning models [12] to estimate vGRF. Martinez-Pascual et al. [15] used five IMU sensors mounted on the foot, lower leg, thigh, hip, and the seventh cervical bone alongside machine learning algorithms in estimating vGRF. Jiang et al. [16] found the optimal placement of IMU sensors for estimating vGRF during overground walking using a random forest regression (RF) algorithm. However, IMU orientation and sensor drift affect the vGRF estimation performances [17], requiring multiple calibrations and complex filter implementations. In addition, current indirect methods of vGRF estimation do not generalize well to unseen user data during testing [15], [16].

To address the problems of current direct and indirect vGRF estimation methods, a novel vGRF estimation method of fusing the center of the pressed sensors (CoPS) and IMU data was proposed. To avoid the influences of drifting errors of pressure sensors, all the pressure sensors on the flexible pressure sensor array were used as pressure switches to detect if the pressure sensor was pressed or not, and CoPS is calculated as the center of all the pressure sensors of the sensor array. In addition to the

arXiv:2501.07748v1 [cs.HC] 13 Jan 2025

popularly used artificial neural networks (ANN) and random forest regression (RF), the performance of bi-directional long-short-term memory (LSTM) in the estimation of vGRF was also evaluated.

The key contributions of this study are summarized as follows:

- 1) Proposed a novel vGRF estimation method using IMU data and newly introduced CoPS data. CoPS is derived from the pressure sensor array by treating the pressure sensors on it as pressure switches, which eliminates the limitations of pressure sensors, such as hysteresis and sensor drift;
- 2) In addition to popularly used machine-learning algorithms – ANN and RF, LSTM was introduced for vGRF estimation. The LSTM model demonstrated superior performance because of its capability to capture temporal dependencies;
- 3) Developed experiments to comprehensively evaluate the effectiveness of the proposed system in intra-participant and inter-participant tests, showing superior generalization performance of the proposed method over the existing state-of-the-art IMU-based vGRF estimation methods.

The remainder of this article is organized as follows. Section II provides an overview of vGRF measurement and estimation techniques. Section III discusses the system design, data processing, and the machine-learning model architecture used in this study. Section IV describes the experiment design and evaluation results. In Section V, we discussed the limitations and future work of the proposed GRF estimation techniques. Finally, the conclusion is given in Section VI.

II. RELATED WORKS

This section focuses on the contributions and limitations of different vGRF measurement and estimation methods.

A. Direct Measurement Methods of vGRF

1) *Traditional Measurement Methods:* Floor-mounted instrumented force plates have been a popular system for gait analysis because of their high accuracy, reliability, and reproducibility in laboratory and clinical settings [1], [4], [6]. However, force plates can only collect data in a single-step manner which makes it challenging to collect a large amount of data [5]. The instrumented treadmill with force plates integrated can address this problem by allowing the recording of multiple steps during cyclic activities [18]. However, instrumented treadmill is designed to be used in controlled environments, limiting their application in real-world settings.

2) *Wearable Sensor-Based Measurement Methods:* Advancements in wearable technologies enable solutions for vGRF measurement in free-living environments. Insole-based pressure sensing systems have been proposed by various studies. For example, pressure sensors based on piezoresistive technologies [7], [9], [10], [19]–[22], capacitive sensing methods [23]–[25], inductive sensors [26], [27], and optical sensors [28], [29] have been explored to develop insole system for measuring vGRF under foot. However, existing flexible pressure sensors used for insole development suffer from

hysteresis problems and drifting errors, which limits their applications in real-world [11], [30]

B. Indirect Estimation Methods of vGRF

1) *Human Biomechanical Methods for vGRF Estimation:* Human biomechanical modeling methods have been proposed as an alternative to estimate vGRF. Optical motion capture systems and IMU-based full-body motion capture systems were used for measuring human body kinematics data [31]. These methods use three-dimensional orientation data, tri-axial linear and rotational displacements, velocity, and acceleration of each human body segment alongside a dynamic human body model to estimate vGRF [14]. However, these methods suffer from accumulated errors during activities such as the double support phase of walking, where a closed-loop mechanical chain is formed. This results in an impossible state for uniquely estimating the vGRF for each foot [12].

2) *Machine Learning Approaches for vGRF Prediction:* Several studies have proposed supervised machine learning and deep learning models to predict vGRF using different sensing technologies [12], [14]. Machine learning models, especially neural networks, can learn complex hidden patterns between input features and dependent variables [32], making them suitable for vGRF prediction tasks. Predicting vGRF without explicitly formulating the human biomechanical models has been made possible by using machine learning models [1].

ANN has shown excellent performances in previous studies for gait analysis tasks [33], [34], and foot shuffling detection [35] using the measured vGRF. Moon et al. [36] proposed an optimized ANN model to predict vGRF using a wearable accelerometer and integrated cameras. Several studies have proposed decision tree algorithms to model vGRF prediction problems due to their robustness to outliers, nonlinear, and unbalanced data [15], [16]. Jiang et al. [16] utilized a RF regressor to predict vGRF for walking activity using a shank-mounted IMU sensor. Although existing machine learning methods yielded better performances for individual subjects, they often performed poorly on unseen subject data and conditions.

3) *Foot Center of Pressure for vGRF Estimation:* The foot Center of Pressure (CoP) is a critical parameter in biomechanics and gait analysis, representing the point of application of the ground reaction force vector [14]. CoP trajectories provide valuable information about balance control, postural stability, and foot function during static and dynamic activities [37]. Several studies have proposed using CoP data to estimate vGRF, aiming to overcome the limitations of laboratory-based force plate systems. Rouhani et al. [38] proposed using CoP data from pressure insoles to estimate complete vGRF during level-ground walking. Jung et al. [39] used CoP data pressure mats alongside joint kinematics to estimate vGRF during walking. Although methods based on CoP data showed promising results in controlled activities, they face challenges in real-world applications due to sensor drift, frequent re-calibration, and poor generalization performances across different users [30].

To address the limitations of existing methods for estimating vGRF, a novel method was proposed by fusing CoPS and IMU data. Three machine learning algorithms – ANN, RF regression models, and LSTM – were evaluated for their performance in vGRF estimation in both intra-participant and inter-participant testing scenarios.

III. MATERIALS AND METHODS

This section specifies details of the smart insole system, the method to extract CoPS, and the algorithms for estimating vGRF.

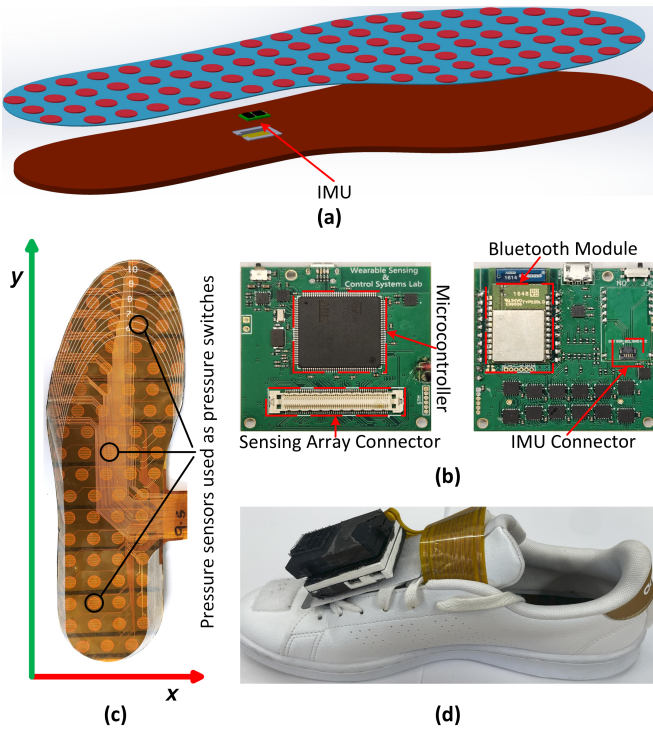


Fig. 1. Overview of the hardware elements of the smart insole system. (a) 3D model of the smart insole with an insole-shaped pressure sensor array on the top, an IMU in the middle, and a flexible substrate on the bottom; (b) The printed circuit board integrates the microcontroller, Bluetooth module, and the connector to the IMU and pressure sensor array; (c) The pressure-sensing array with pressure sensors uniformly distributed on it; (d) Assembled shoes with the smart insole system.

A. Smart Insole System

Fig. 1 shows the smart insole’s hardware systems for signal acquisition and wireless data transmission. As shown in Fig. 1(c), an insole-shaped pressure sensing array, is used for measuring the plantar pressure signal [10]. The sensing array utilized a customizable design to reduce the manufacturing cost, which can be trimmed to fit foot sizes from 5.5 U.S. to 14 U.S. Fig. 1(a) shows the structure of the smart insole, with the pressure sensor array on the top, an IMU module in the middle, and a 3D printed flexible substrate on the bottom. The IMU placed at the midfoot region was used to estimate the foot’s three-dimensional acceleration, angular velocity, and angle. The smart insole system is powered by a 3.7 V, 1000 mAh battery that is mounted on the shoe using a custom 3D-printed housing attachment (Fig. 1(d)).

B. Center of the Pressed Sensor Measurement

Fig. 1(c) shows the pressure sensing array made from a flexible printed circuit board. The sensing array comprises 96 individual sensors uniformly distributed on the foot plantar surface. Calculating the CoPS requires using the pressure sensors as pressure switches to detect if an individual pressure sensor is pressed. Based on our previous study, an adaptive threshold was used to accurately determine the sensor’s ON and OFF states [7], [9]. The adaptive threshold can be estimated using equation (1).

$$AT_I = \frac{1}{n_{swing}} \sum_{k=1}^{n_{swing}} Pressure_{k_I} + 3 * \sigma_{swing}. \quad (1)$$

Where AT_I indicates the adaptive threshold of sensor I ($I = 1, 2, 3, \dots, 96$), $Pressure_{k_I}$ is the pressure measured by the individual sensor I in the sensing array, n_{swing} is the total number of swing pressure samples of sensor I collected when the foot is off the ground, and σ_{swing} is the standard deviation of the swing pressure samples. Equation (2) shows the estimation of the sensor states:

$$S_I = \begin{cases} 1, & Pressure_I \geq AT_I \\ 0, & \text{otherwise} \end{cases} \quad (2)$$

where S_I indicates the sensor state of sensor I , and $Pressure_I$ indicates the pressure measured by sensor I in the sensing array. CoPS was measured by using the sensor states and their respective coordinates, as shown in equation (3).

$$\begin{cases} CoPS_x = \frac{\sum_{j=1}^I x_j \cdot s_j}{\sum_{j=1}^I s_j} \\ CoPS_y = \frac{\sum_{j=1}^I y_j \cdot s_j}{\sum_{j=1}^I s_j} \end{cases} \quad (3)$$

where $CoPS_x$ and $CoPS_y$ indicate the anterior-posterior and medial-lateral $CoPS$, respectively, x_j and y_j are the coordinates of the sensors j , s_j is the state of the sensor j , and I is the total number of the sensors.

C. Data Processing

Fig. 2 illustrates the detailed data processing pipeline and the inputs to the machine learning models used in this study. First, the vGRF data measured by the instrumented treadmill underwent normalization using the participants’ body weight (BW). The normalized vGRF serves as the ground truth for the machine learning regression models. The foot contact event, which can be accurately detected by both the instrumented treadmill and the smart insole, was used to synchronize the data from both systems. The pressure sensors on the pressure sensor arrays were used as pressure switches, and the CoPS can be estimated with method shown in section III-B. To obtain the foot angles, we utilized the orientation filter developed in [40], using the data acquired from the linear acceleration and the angular velocities of the IMU sensors integrated into the insoles.

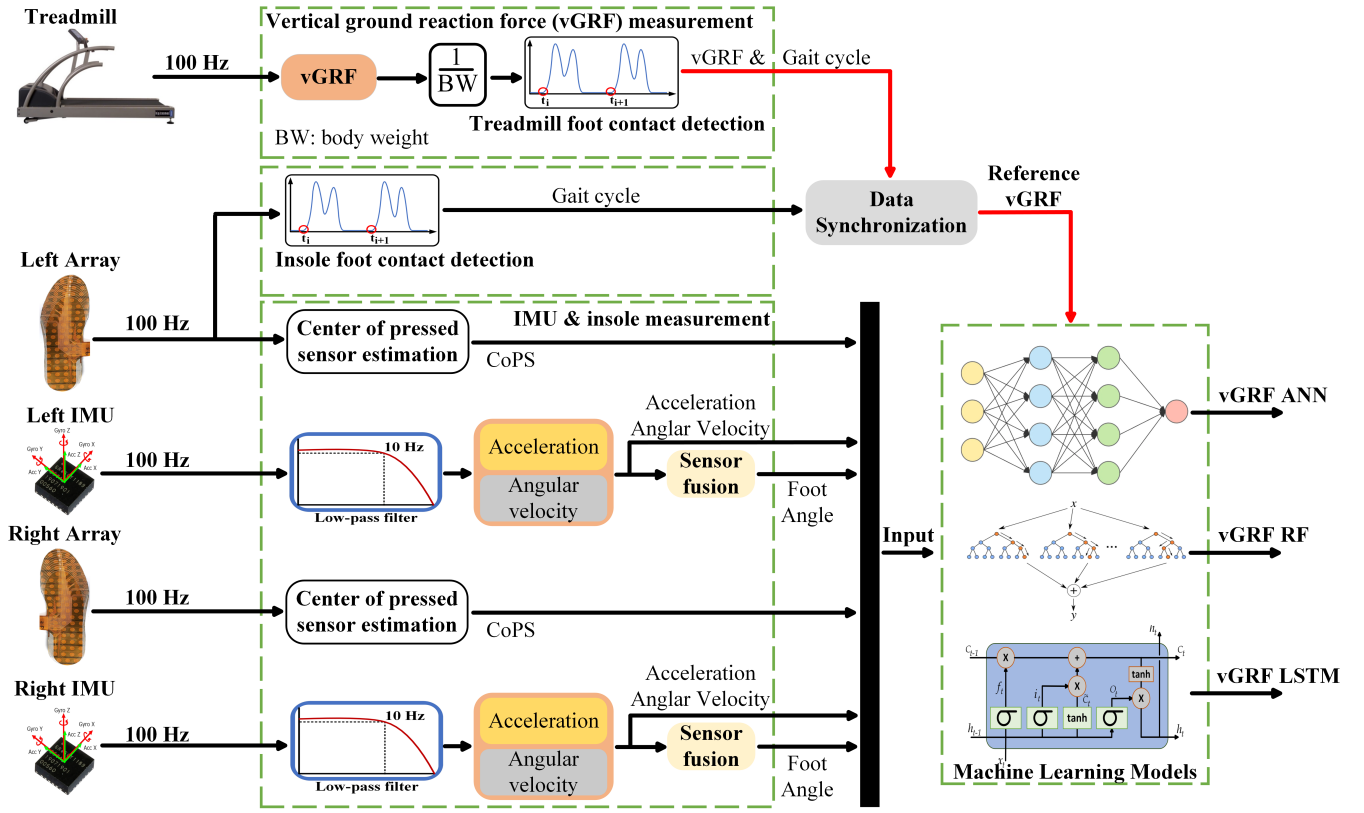


Fig. 2. An overview of the process for data collection, data processing, vGRF estimation.

The vGRF, CoPS, and IMU data of each gait cycle (determined by two consecutive heel contact events) was padded into a window of two seconds [41]. All the padded data were added to the swing phase of each gait cycle. The two-second window was used because previous studies have shown that the two-second window size provides the best trade-off between speed and accuracy [42]. All the processed data were further normalized to a uniform range between 0 and 1 before feeding them as inputs to the machine learning models for training and testing.

The estimated vGRF from the ANN and RF models were filtered using a zero-phase low-pass filter at a 10 Hz frequency, as the majority of the spectral component of ground reaction forces is contained below 10 Hz [43]. The weight acceptance peak (WAP) and the push-off peak (POP) were detected by searching the local maxima in each stance cycle’s first and second halves. The WAP determines the local maximum in the first half of the stance cycle, while the local maximum in the second half of the stance cycle corresponds to the POP [7].

D. Machine Learning Algorithms for vGRF Estimation

The vGRF estimation is a regression task. In this study, three machine-learning regression model architectures were trained to estimate the vGRF. We chose RF regression model and the ANN models due to their popularity in estimating vGRF and analyzing gait data [15], [16]. Additionally, bi-directional LSTM networks were chosen to predict vGRF due to their

ability to capture temporal dependencies in both forward and backward directions. This bidirectional approach allows the model to leverage both past and future context at each time step, making it particularly suitable for analyzing the complex, cyclic nature of gait dynamics. LSTMs’ capacity to model long-term dependencies and their robustness to vanishing gradient problems further enhance their effectiveness in predicting time-dependent force patterns.

The ANN, RF, and LSTM models were trained using the PyTorch Python Library (PyTorch Foundation). We used an ANN model with one input layer with the number of neurons matching the input feature size, five hidden layers with 20 neurons, and an output layer with one neuron. The RF training was performed using 200 decision trees and two leaves. The output of the RF model was majority-voted from the results produced by the individual trees. For the LSTM model, a four-layer bidirectional LSTM network with 128 units with dropout regularization was utilized to reduce overfitting. For all three models (ANN, RF, and LSTM), the RMSE loss function was used.

E. Model Training and Testing

For the training of the selected machine learning algorithms (ANN, RF, and LSTM), we assessed the model performances using two model training topologies – intra-participant and inter-participant training methods. Intra-participant training and testing, also called same-participant testing, involves using datasets from the same user to train and evaluate the model

performance. In this study, 70% of the data from all three walking speeds of a participant is used for training, while the rest is used to evaluate the model performance on unseen data from the same user. The intra-participant testing is repeated for all participants' datasets using all three walking speeds. The model accuracy is then calculated and averaged for each walking speed across all participants.

In contrast, inter-participant testing, also known as leave-one-subject-out cross-validation, involves using all the data from a group of participants to train the machine learning model, while another dataset from a group that was not part of the training data is used to evaluate the model performance. In this study, data from seven subjects is used for training, while the data from the remaining one subject is used to test the model. This process is repeated until data from each participant has been used to test the model performance. The model accuracy is then calculated and averaged for each walking speed across all participants. The inter-participant testing evaluates the generalization capabilities of the model to an unseen population.

To analyze the effectiveness of the newly introduced CoPS data and the fusion of CoPS and IMU data on the estimated vGRF, We developed three model training sets for each machine learning algorithm.

- Training 1 (T1): IMU features – three-axis linear acceleration, three-axis angular velocity, and three-axis foot angle data for both feet were included as inputs to the machine-learning models.
- Training 2 (T2): CoPS features – anterior-posterior and medial-lateral CoPS data for both feet were included as inputs to the machine-learning models.
- Training 3 (T3): IMU and CoPS features – data from both the IMU and CoPS from both feet were combined as the inputs to the model.

F. Model Performance Evaluation

This study utilized multiple performance metrics, and the performance achieved by the vGRF estimation methods was evaluated as follows:

- **Root mean squared error (RMSE):** The RMSE measures the distance between the estimated and reference vGRF trajectories. We selected the RMSE because it penalizes larger errors, resulting in better vGRF peak estimation.
- **Normalized Root mean squared error (NRMSE):** The NRMS normalizes the RMSE by dividing the RMSE by the range of the reference vGRF: equation (4), as defined by Mentaschi et al. in [44]. A lower NRMSE in the reconstruction of vGRF indicates better model performance.

$$\text{NRMSE} = \frac{\text{RMSE}}{\max(\text{vGRF}_{\text{ref}}) - \min(\text{vGRF}_{\text{ref}})} \quad (4)$$

- **Correlation coefficient (R):** R in this study measured the similarity estimated vGRF and the reference vGRF measured by the treadmill. The values of ρ range from

-1.0 to 1.0, where $R = 1.0$ represents a perfectly positive correlation, $R = 0.0$ implies no linear relationship between the reference measurement and the estimated vGRF, and $R = -1.0$ results in a perfectly negative correlation. In this study, Pearson's correlation coefficient was used as a metric, and the closer R gets to 1.0, the better.

- **WAP and POP error:** A lower RMSE between the reference and estimated vGRF peaks (WAP and POP) results in a better model performance. WAP and POP are the local maxima in the first and second halves of each vGRF stance phase, respectively [7].
- **WAP and POP delay:** The timing occurrence of the detected WAP and POP were also recorded, and their respective delay or advance errors were estimated. A delay or advance close to 0% of the gait cycle implies a better performance of the model.

IV. EXPERIMENTS AND RESULTS

A. Experimental Setup



Fig. 3. The experiment setup. The participant wears a pair of smart insole and walks on a force-plate instrumented treadmill.

Fig. 3 shows the experiment setup. An instrumented treadmill with embedded force plates (h/p/cosmos GaitWay III) was used to measure the reference vGRF with a sample rate of 100 Hz during the experiment. Eight healthy adults recruited from the local university population participated in this study. The heights range between 1.66 m to 1.82 m (173 ± 5.6 cm), with foot lengths ranging from 25 cm to 27.3 cm (26.19 ± 0.65 cm) and body weights between 66.5 kg and 82 kg (75.69 ± 6.24 kg). IRB approval and written informed consent from all the participants were obtained for this study. During the experiment, each participant wore a pair of smart insole and walked on the treadmill at three speeds: 0.7 m/s, 1.0 m/s, and 1.4 m/s. The speeds cover the range of average gait speeds for adult humans [45]. Each trial lasted for 90 seconds, progressing from low to high speeds with a two-minute rest between each trial. Before data collection, participants were given time to warm up and become comfortable on the treadmill. The pressure sensor array and inertial measurement

TABLE I
MEAN AND STANDARD DEVIATION OF INTRA-PARTICIPANT TESTING RMSE FOR THE ANN, RF, AND LSTM MODELS.

Model	Features	RMSE (BW)			
		Global	0.7 m/s	1.0 m/s	1.4 m/s
ANN	T1	0.058 ± 0.014	0.054 ± 0.014	0.057 ± 0.021	0.063 ± 0.015
	T2	0.064 ± 0.015	0.062 ± 0.015	0.054 ± 0.020	0.062 ± 0.016
	T3	0.056 ± 0.014	0.049 ± 0.013	0.054 ± 0.020	0.062 ± 0.016
RF	T1	0.033 ± 0.004	0.032 ± 0.006	0.032 ± 0.007	0.034 ± 0.007
	T2	0.037 ± 0.005	0.038 ± 0.008	0.034 ± 0.010	0.041 ± 0.005
	T3	0.029 ± 0.003	0.025 ± 0.004	0.028 ± 0.008	0.033 ± 0.006
LSTM	T1	0.029 ± 0.005	0.028 ± 0.006	0.027 ± 0.007	0.029 ± 0.004
	T2	0.027 ± 0.006	0.028 ± 0.007	0.025 ± 0.007	0.027 ± 0.006
	T3	0.024 ± 0.003	0.023 ± 0.006	0.023 ± 0.003	0.026 ± 0.004

Note: T1 corresponds to IMU features only, T2 to CoPS features only, and T3 to data fusion of IMU and CoPS features. Global RMSE is the average of all participants' RMSE across all gait speeds.

TABLE II
MEAN AND STANDARD DEVIATION OF INTER-PARTICIPANT TESTING RMSE FOR THE ANN, RF, AND LSTM MODELS.

Model	Features	RMSE (BW)			
		Global	0.7 m/s	1.0 m/s	1.4 m/s
ANN	T1	0.088 ± 0.017	0.076 ± 0.017	0.082 ± 0.031	0.099 ± 0.014
	T2	0.089 ± 0.015	0.082 ± 0.019	0.076 ± 0.025	0.099 ± 0.009
	T3	0.082 ± 0.017	0.069 ± 0.012	0.077 ± 0.027	0.092 ± 0.018
RF	T1	0.076 ± 0.021	0.073 ± 0.029	0.074 ± 0.023	0.077 ± 0.023
	T2	0.077 ± 0.020	0.080 ± 0.029	0.068 ± 0.027	0.081 ± 0.019
	T3	0.070 ± 0.019	0.062 ± 0.018	0.067 ± 0.025	0.078 ± 0.025
LSTM	T1	0.050 ± 0.005	0.043 ± 0.011	0.047 ± 0.011	0.052 ± 0.007
	T2	0.047 ± 0.008	0.040 ± 0.008	0.040 ± 0.014	0.050 ± 0.013
	T3	0.044 ± 0.005	0.038 ± 0.009	0.043 ± 0.010	0.044 ± 0.006

Note: T1 corresponds to IMU features only, T2 to CoPS features only, and T3 to data fusion of IMU and CoPS features. Global RMSE is the average of all participants' RMSE across all gait speeds.

unit integrated into the smart insole were recorded at a 50 Hz sampling rate and upsampled to 100 Hz to match the treadmill.

All eight participants completed the entire data collection protocol. A total of 27,000 IMU and CoPS samples were collected from each participant across 3 experiment trials, resulting in 216,000 total samples collected from all eight participants. We excluded some gait cycles from the data due to incorrect/missing recordings (e.g., on some occasions when the participants walked on a single force plate embedded with the treadmill).

B. Results

After training all three machine learning models (ANN, RF, and LSTM) for all three training sets (T1, T2, and T3), we evaluated the accuracy of the models with the test data for both the intra-participant and the inter-participant training methods. The RMSE, NRMSE, R, WAP, and POP errors were calculated for each gait cycle. The mean and standard deviations of the RMSE for each machine-learning algorithm are shown in Table I and Table II for the intra-participant and inter-participant testing, respectively.

The two-way ANOVA obtained for the intra-participant testing showed that there were statistically significant effects of the machine-learning algorithm type and the input feature type on the RMSE (algorithm, $F(22) = 180.20$, $p < 0.001$; feature, $F(22) = 7.56$, $p = 0.0041$) for all gait speeds. The ANOVA results showed that the choice of algorithms and the types of input features used to train the models individually affect the accuracy and reliability of the vGRF estimation. In the pairwise comparisons, significant differences were observed between ANN and RF ($p < 0.0001$), ANN and LSTM ($p < 0.0001$), and RF and LSTM ($p = 0.02$) machine-learning algorithms on the estimated vGRF accuracy (RMSE). Similarly, the two-way ANOVA of the RMSE obtained for the inter-participant testing showed that there was a significant effect of the algorithm type on the RMSE ($F(22) = 54.31$, $p < 0.001$). The post hoc analysis showed that there were significant differences between the ANN and RF ($p = 0.025$), ANN and LSTM ($p < 0.0001$), and RF and LSTM ($p < 0.0001$) machine-learning algorithms on the estimated vGRF accuracy (RMSE). These results highlighted the superior performance of the LSTM model over the other models. Further analysis showed that CoPS (T2) has better performance than IMU (T1)

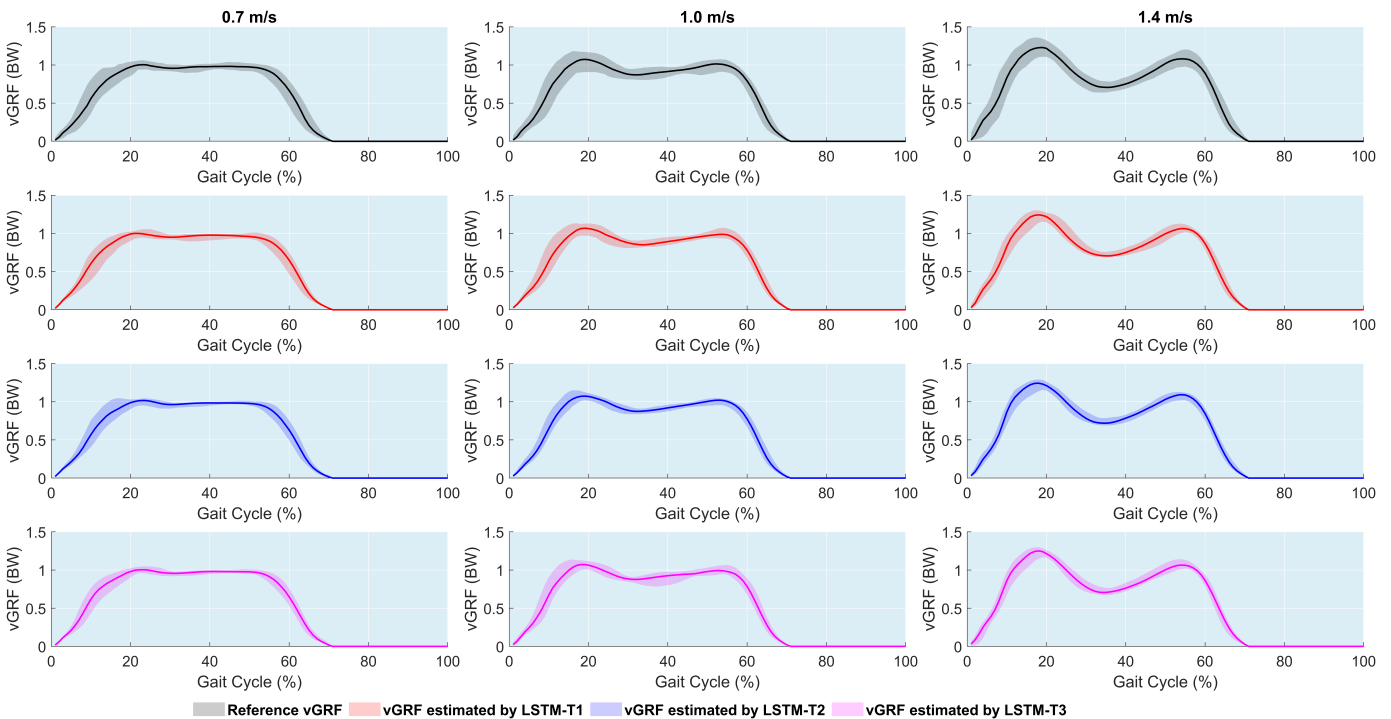


Fig. 4. Epoch graphs of the measured and estimated vGRF for the inter-participant testing method at different walking speeds. The median value has been plotted with lines, while the values between the 2.5th and 97.5th percentiles are shaded.

data and the fusion of CoPS and IMU features (T3) resulted in the best accuracy for LSTM models.

As the LSTM models with the IMU features, CoPS features, and the fusion of both the IMU and CoPS features have the best performances for the intra-participant and inter-participant test cases, these three LSTM models are further evaluated with NRMSE, correlation, and the accuracy of WAP and POP.

Figure 4 shows the reference vGRF, the vGRF estimated with the LSTM-T1, LSTM-T2, and LSTM-T3. The solid continuous line indicates the median value of the vGRF for all gait cycles and the shaded region corresponds to the values between 2.5th and 97.5th percentiles of the vGRF signals. Table III shows the correlation coefficient (R) and NRMSE between the reference and estimated vGRF with the selected models (LSTM-T1, LSTM-T2, and LSTM-T3) for the intra-participant and inter-participant testing. Table IV and Table V show the mean magnitude errors and delays of the estimated vGRF peaks (WAP and POP). Overall, the LSTM-T2 has a better performance than LSTM-T1 which shows the advantage of the CoPS over IMU in estimating vGRF. For most cases, LSTM-T3 has the best performance which shows the advantage of fusing CoPS and IMU data in estimating vGRF.

V. DISCUSSION

This study introduced new data – CoPS for vGRF estimating and showed its advantage over existing IMU-based methods. Additionally, other than popularly used ANN and RF, this study also evaluated LSTM and showed its advantage in vGRF estimation.

TABLE III
CORRELATION (R) AND NORMALIZED RMSE (NRMSE) RESULTS BETWEEN THE REFERENCE vGRF AND THE ESTIMATED vGRF BY THE LSTM MODELS FOR THE INTRA-PARTICIPANT AND INTER-PARTICIPANT TESTING.

LSTM	Speed (m/s)	Intra-Participant		Inter-Participant	
		R	NRMSE (% BW)	R	NRMSE (% BW)
T1	0.7	0.9950	2.66	0.9886	4.05
	1.0	0.9962	2.30	0.9885	3.98
	1.4	0.9959	2.16	0.9869	3.85
	Global	0.9958	2.13	0.9878	3.64
T2	0.7	0.9951	2.62	0.9902	3.76
	1.0	0.9968	2.10	0.9883	3.99
	1.4	0.9965	1.99	0.9880	3.64
	Global	0.9964	1.96	0.9888	3.46
T3	0.7	0.9966	2.19	0.9911	3.55
	1.0	0.9974	1.91	0.9900	3.67
	1.4	0.9969	1.89	0.9906	3.27
	Global	0.9970	1.79	0.9905	3.22

Note: T1 corresponds to the LSTM model trained with the IMU feature, T2 to the LSTM model with the CoPS feature, and T3 to the LSTM model with the data fusion of IMU and CoPS features.

Through comparing the performances of all nine trained models (ANN, RF, and LSTM models for T1, T2, and T3 features), some differences can be observed between them for the intra- and inter-participant testing. The RMSE of the ANN model ranges between 0.049 BW and 0.063 BW, which is about twice the RMSE of RF and LSTM models

TABLE IV
WAP AND POP ERRORS OBTAINED WITH THE LSTM MODELS FOR THE INTRA-PARTICIPANT AND INTER-PARTICIPANT TESTING.

LSTM	Speed (m/s)	Intra-participant		Inter-participant	
		WAP (BW)	POP (BW)	WAP (BW)	POP (BW)
T1	0.7	0.023	0.017	0.026	0.021
	1.0	0.032	0.021	0.055	0.033
	1.4	0.032	0.024	0.059	0.039
	Global	0.030	0.022	0.051	0.033
T2	0.7	0.017	0.014	0.021	0.014
	1.0	0.024	0.014	0.059	0.027
	1.4	0.028	0.021	0.055	0.035
	Global	0.024	0.017	0.050	0.028
T3	0.7	0.016	0.012	0.021	0.019
	1.0	0.020	0.014	0.049	0.021
	1.4	0.026	0.021	0.051	0.031
	Global	0.022	0.017	0.044	0.025

Note: T1 corresponds to the LSTM model trained with the IMU feature, T2 to the LSTM model with the CoPS feature, and T3 to the LSTM model with the data fusion of IMU and CoPS features.

TABLE V
WAP AND POP TIMING DELAY OBTAINED WITH THE LSTM MODELS FOR THE INTRA-PARTICIPANT AND INTER-PARTICIPANT TESTING.

LSTM	Speed (m/s)	Intra-participant		Inter-participant	
		WAP (% GC)	POP (% GC)	WAP (% GC)	POP (% GC)
T1	0.7	1.6	4.0	3.3	4.4
	1.0	1.3	2.1	2.0	2.7
	1.4	0.9	0.7	1.3	1.2
	Global	1.2	1.9	2.0	2.4
T2	0.7	2.7	3.3	2.5	4.2
	1.0	1.3	2.0	1.9	2.2
	1.4	0.8	0.7	1.1	1.0
	Global	1.4	1.7	1.7	2.1
T3	0.7	2.9	3.9	2.3	4.3
	1.0	1.2	1.8	1.6	2.7
	1.4	0.8	0.6	1.0	0.9
	Global	1.4	1.8	1.5	2.3

Note: T1 corresponds to the LSTM model trained with the IMU feature, T2 to the LSTM model with the CoPS feature, and T3 to the LSTM model with the data fusion of IMU and CoPS features. GC – gait cycle.

(0.023 BW to 0.041 BW) during the intra-participant testing. This can be attributed to the inability of the ANN model to extract the temporal dependency in the walking gait data and a similar problem was reported in [15]. Despite the comparable performance of the RF model with the LSTM models for the intra-participant testing, there seems to be a significant performance degradation during inter-participant testing (Table I and Table II). The performance degradation of the RF models can be attributed to model overfitting during training, a common problem with algorithms based on decision trees [46].

The ANOVA analysis for the intra-participant and inter-participant testing reveals that the LSTM model consistently outperforms the ANN and RF models, as evidenced by lower RMSE, NRMSE, and higher correlation coefficients. This performance can be attributed to the bi-directional LSTM’s architecture, which effectively captures temporal dependencies inherent in gait data in forward and reverse directions. The superior accuracy and reduced error rates suggest that the LSTM model is particularly well-suited for applications requiring precise vGRF estimation.

TABLE VI
INTER-PARTICIPANT PERFORMANCE COMPARISON OF vGRF ESTIMATION WITH EXISTING METHODS.

Author	Year	Model	RMSE (BW)	NRMSE (%BW)
Our method	2024	LSTM	0.044	3.22
Jiang et al. [16]	2020	RF	0.100	7.15
Martinez-Pascual et al. [15]	2023	ANN	0.074	6.84
Martinez-Pascual et al. [15]	2023	RF	0.077	7.27
Karatsidis et al. [31]	2017	HBM/NE	0.063	5.30

Note: The unit of RMSE is body weight (BW), NRMSE – percent of the body weight (%BW). HBM – Human Biomechanical model, and NE – Newton-Euler Equation.

The proposed vGRF estimation methods proposed in this study outperformed the existing state-of-the-art solutions. Table VI shows the comparison between our proposed method and existing methods reported in the literature. Martinez-Pascual et al. [15] investigated using an ANN and RF to estimate vGRF with five IMU sensors during walking. The best RMSE and NRMSE achieved were 0.074 BW and 6.84% BW, respectively. Jiang et al. [16] used RF to achieve RMSE and NRMSE of 0.1 BW and 7.15% BW, respectively. Karatsidis et al. [31] used human biomechanical models and Newton-Euler’s methods to achieve 0.063 BW and 5.3% BW for RMSE and NRMSE, respectively. The method proposed in this study, which estimates vGRF with LSTM and CoPS and IMU data, achieved 0.044 BW and 3.22% BW for RMSE and NRMSE, respectively. This result outperformed vGRF estimation methods previously reported in the literature [12], [14].

This study was limited to the vGRF estimation for only healthy adult populations. Variations in age, foot shape, and gait pathologies might introduce complexities that the current method may not fully capture. Future works will explore a wider population demographic, including populations with a wider range of ages, heights, sexes, and distinct gait patterns, such as elderly individuals or those with neurological conditions.

VI. CONCLUSION

This paper presents a method of estimating the vGRF with CoPS and IMU. Three machine learning models: ANN, RF, and LSTM were evaluated for vGRF estimation. The results showed that CoPS has better performance than IMU and LSTM has better performance over popularly used ANN and

RF. The LSTM model trained with the fusion of CoPS and IMU data achieved the best performance when compared with existing state-of-the-art solutions. The results of this study show the feasibility of using the CoPS and IMU for accurate vGRF estimation during walking.

ACKNOWLEDGMENTS

We would like to express our gratitude to Professor Dain LaRoche and the Kinesiology Department of the University of New Hampshire for providing access to the instrumented treadmill, which was essential for conducting experiments and collecting ground truth vGRF data.

REFERENCES

- [1] A. Ancillao and A. Ancillao, "Stereophotogrammetry in functional evaluation: history and modern protocols," *Modern functional evaluation methods for muscle strength and gait analysis*, pp. 1–29, 2018.
- [2] D. Chen, J. Chen, H. Jiang, and M.-C. Huang, "Risk factors identification for work-related musculoskeletal disorders with wearable and connected gait analytics system," in *2017 IEEE/ACM International Conference on Connected Health: Applications, Systems and Engineering Technologies (CHASE)*. IEEE, 2017, pp. 330–339.
- [3] D. Chen, Y. Cai, J. Cui, J. Chen, H. Jiang, and M.-C. Huang, "Risk factors identification and visualization for work-related musculoskeletal disorders with wearable and connected gait analytics system and kinect skeleton models," *Smart Health*, vol. 7, pp. 60–77, 2018.
- [4] M. Brandes, R. Schomaker, G. Möllenhoff, and D. Rosenbaum, "Quantity versus quality of gait and quality of life in patients with osteoarthritis," *Gait & Posture*, vol. 28, no. 1, pp. 74–79, 2008. [Online]. Available: <https://www.sciencedirect.com/science/article/pii/S0966636207002597>
- [5] A. Stacoff, I. A. K. de Quervain, G. Luder, R. List, and E. Stüssi, "Ground reaction forces on stairs: Part ii: Knee implant patients versus normals," *Gait & Posture*, vol. 26, no. 1, pp. 48–58, 2007. [Online]. Available: <https://www.sciencedirect.com/science/article/pii/S0966636206001664>
- [6] G. Lee and A. E. Park, "Development of a more robust tool for postural stability analysis of laparoscopic surgeons," *Surgical Endoscopy*, vol. 22, pp. 1087–1092, 2008. [Online]. Available: <https://doi.org/10.1007/s00464-007-9664-3>
- [7] D. Chen, Y. Cai, X. Qian, R. Ansari, W. Xu, K.-C. Chu, and M.-C. Huang, "Bring gait lab to everyday life: Gait analysis in terms of activities of daily living," *IEEE Internet of Things Journal*, vol. 7, no. 2, pp. 1298–1312, 2020.
- [8] A. Khandakar, S. Mahmud, M. E. H. Chowdhury, M. B. I. Reaz, S. Kiranyaz, Z. B. Mahbub, S. H. M. Ali, A. A. A. Bakar, M. A. Ayari, M. Alhatou, M. Abdul-Moniem, and M. A. A. Faisal, "Design and implementation of a smart insole system to measure plantar pressure and temperature," *Sensors*, vol. 22, no. 19, 2022. [Online]. Available: <https://www.mdpi.com/1424-8220/22/19/7599>
- [9] D. Chen, N. Ghoreishi, F. Olugbon, S. Ansah, M.-C. Huang, and Q. Yu, "Optimal pressure sensor locations in smart insoles for heel-strike and toe-off detection," in *2022 IEEE Biomedical Circuits and Systems Conference (BioCAS)*, 2022, pp. 458–461.
- [10] D. Chen, Y. Cai, and M.-C. Huang, "Customizable pressure sensor array: Design and evaluation," *IEEE Sensors Journal*, vol. 18, no. 15, pp. 6337–6344, 2018.
- [11] M. Y. Saadeh, T. D. Carambat, and A. M. Arrieta, "Evaluating and modeling force sensing resistors for low force applications," in *Smart Materials, Adaptive Structures and Intelligent Systems*, vol. 58264. American Society of Mechanical Engineers, 2017, p. V002T03A001.
- [12] A. Ancillao, S. Tedesco, J. Barton, and B. O'Flynn, "Indirect measurement of ground reaction forces and moments by means of wearable inertial sensors: A systematic review," *Sensors*, vol. 18, no. 8, p. 2564, 2018.
- [13] S. Tedesco, A. Urru, A. Clifford, and B. O'Flynn, "Experimental validation of the tyndall portable lower-limb analysis system with wearable inertial sensors," *Procedia Engineering*, vol. 147, pp. 208–213, 2016.
- [14] E. Shahabpoor and A. Pavic, "Measurement of walking ground reactions in real-life environments: A systematic review of techniques and technologies," *Sensors*, vol. 17, no. 9, p. 2085, 2017.
- [15] D. Martínez-Pascual, J. M. Catalán, A. Blanco-Ivorra, M. Sanchís, F. Arán-Ais, and N. García-Aracil, "Estimating vertical ground reaction forces during gait from lower limb kinematics and vertical acceleration using wearable inertial sensors," *Frontiers in Bioengineering and Biotechnology*, vol. 11, p. 1199459, 2023.
- [16] X. Jiang, C. Napier, B. Hannigan, J. J. Eng, and C. Menon, "Estimating vertical ground reaction force during walking using a single inertial sensor," *Sensors*, vol. 20, no. 15, p. 4345, 2020.
- [17] T. Tan, D. P. Chiasson, H. Hu, and P. B. Shull, "Influence of imu position and orientation placement errors on ground reaction force estimation," *Journal of biomechanics*, vol. 97, p. 109416, 2019.
- [18] L. van Gelder, A. T. Booth, I. van de Port, A. I. Buizer, J. Harlaar, and M. M. van der Krogt, "Real-time feedback to improve gait in children with cerebral palsy," *Gait & posture*, vol. 52, pp. 76–82, 2017.
- [19] D. Chen, G. Asaekheybari, H. Chen, W. Xu, and M.-C. Huang, "Ubiquitous fall hazard identification with smart insole," *IEEE Journal of Biomedical and Health Informatics*, vol. 25, no. 7, pp. 2768–2776, 2021.
- [20] T. Liu, Y. Inoue, and K. Shibata, "A wearable ground reaction force sensor system and its application to the measurement of extrinsic gait variability," *Sensors*, vol. 10, no. 11, pp. 10240–10255, 2010.
- [21] "Measurement specialties. pressure sensors, position sensors, temperature sensors," accessed on April 14, 2024. [Online]. Available: <http://www.meas-spec.com/>
- [22] "Pcb piezotronics, inc. sensors that measure up!" accessed on April 12, 2024. [Online]. Available: <http://www.pcb.com/>
- [23] "Novel quality in measurement," accessed on April 13, 2024. [Online]. Available: <http://www.novel.de/>
- [24] J. Mertodikromo, F. Zorin, and C. J. Lee, "A low-profile shear force sensor for wearable applications," *IEEE Sensors Journal*, vol. 20, no. 18, pp. 10453–10459, 2020.
- [25] J. Tang, D. L. Bader, D. Moser, D. J. Parker, S. Forghany, C. J. Nester, and L. Jiang, "A wearable insole system to measure plantar pressure and shear for people with diabetes," *Sensors*, vol. 23, no. 6, p. 3126, 2023.
- [26] T. Liu, Y. Inoue, and K. Shibata, "A small and low-cost 3-d tactile sensor for a wearable force plate," *IEEE Sensors Journal*, vol. 9, no. 9, pp. 1103–1110, 2009.
- [27] L. Wang, D. Jones, A. Jones, G. J. Chapman, H. J. Siddle, D. Russell, A. Alazmani, and P. R. Culmer, "A portable insole system to simultaneously measure plantar pressure and shear stress," *IEEE Sensors Journal*, vol. 22, no. 9, pp. 9104–9113, 2022.
- [28] M. A. McGeehan, S. S. Kariyott, M. E. Hahn, D. C. Morgenroth, and K. G. Ong, "An optoelectronics-based sensor for measuring multi-axial shear stresses," *IEEE Sensors Journal*, vol. 21, no. 22, pp. 25641–25648, 2021.
- [29] C. Tavares, F. Leite, M. D. F. Domingues, T. Paixao, N. Alberto, A. Ramos, H. Silva, and P. F. D. C. Antunes, "Optically instrumented insole for gait plantar and shear force monitoring," *IEEE Access*, vol. 9, pp. 132480–132490, 2021.
- [30] A. H. A. Razak, A. Zayegh, R. K. Begg, and Y. Wahab, "Foot plantar pressure measurement system: A review," *Sensors*, vol. 12, no. 7, pp. 9884–9912, 2012.
- [31] A. Karatsidis, G. Bellusci, H. M. Schepers, M. De Zee, M. S. Andersen, and P. H. Veltink, "Estimation of ground reaction forces and moments during gait using only inertial motion capture," *Sensors*, vol. 17, no. 1, p. 75, 2016.
- [32] J. S. Almeida, "Predictive non-linear modeling of complex data by artificial neural networks," *Current opinion in biotechnology*, vol. 13, no. 1, pp. 72–76, 2002.
- [33] R. Lafuente, J. Belda, J. Sanchez-Lacuesta, C. Soler, and J. Prat, "Design and test of neural networks and statistical classifiers in computer-aided movement analysis: a case study on gait analysis," *Clinical Biomechanics*, vol. 13, no. 3, pp. 216–229, 1998.
- [34] F. J. Wouda, M. Giuberti, G. Bellusci, E. Maartens, J. Reenalda, B.-J. F. Van Beijnum, and P. H. Veltink, "Estimation of vertical ground reaction forces and sagittal knee kinematics during running using three inertial sensors," *Frontiers in physiology*, vol. 9, p. 218, 2018.
- [35] S. Ansah, F. Olugbon, S. Arthanat, D. LaRoche, and D. Chen, "Smart insole based shuffling detection system for improved gait analysis in parkinson's disease," in *2023 IEEE 19th International Conference on Body Sensor Networks (BSN)*. IEEE, 2023, pp. 1–4.
- [36] J. Moon, T. Kim, S. Lee, G. A. Ruiz Sanchez, and S. Kim, "Prediction of ground reaction forces by combination of kinematic variables during gait: Based on optimized artificial neural network algorithm," *Available at SSRN 4662667*, 2024.

- [37] V. Lugade and K. Kaufman, "Center of pressure trajectory during gait: a comparison of four foot positions," *Gait & posture*, vol. 40, no. 4, pp. 719–722, 2014.
- [38] H. Rouhani, J. Favre, X. Crevoisier, and K. Aminian, "Ambulatory assessment of 3d ground reaction force using plantar pressure distribution," *Gait & posture*, vol. 32, no. 3, pp. 311–316, 2010.
- [39] Y. Jung, M. Jung, K. Lee, and S. Koo, "Ground reaction force estimation using an insole-type pressure mat and joint kinematics during walking," *Journal of biomechanics*, vol. 47, no. 11, pp. 2693–2699, 2014.
- [40] S. Madgwick *et al.*, "An efficient orientation filter for inertial and inertial/magnetic sensor arrays," *Report x-io and University of Bristol (UK)*, vol. 25, pp. 113–118, 2010.
- [41] S. Ansah and D. Chen, "Wearable-gait-analysis-based activity recognition: A review," *International Journal on Smart Sensing and Intelligent Systems*, vol. 15, no. 1, 2022.
- [42] O. Banos, J.-M. Galvez, M. Damas, H. Pomares, and I. Rojas, "Window size impact in human activity recognition," *Sensors*, vol. 14, no. 4, pp. 6474–6499, 2014. [Online]. Available: <https://www.mdpi.com/1424-8220/14/4/6474>
- [43] J. T. Blackburn, B. G. Pietrosimone, M. S. Harkey, B. A. Luc, and D. N. Pamukoff, "Comparison of three methods for identifying the heelstrike transient during walking gait," *Medical Engineering & Physics*, vol. 38, no. 6, pp. 581–585, 2016.
- [44] L. Mentaschi, G. Besio, F. Cassola, and A. Mazzino, "Why nrmse is not completely reliable for forecast/hindcast model test performances," in *Geophysical Research Abstracts*, vol. 15, 2013.
- [45] D. Weber, "Differences in physical aging measured by walking speed: evidence from the english longitudinal study of ageing," *BMC geriatrics*, vol. 16, pp. 1–9, 2016.
- [46] T. Dietterich, "Overfitting and undercomputing in machine learning," *ACM computing surveys (CSUR)*, vol. 27, no. 3, pp. 326–327, 1995.